Comparison Study of Microstructure and Phase Evolution in Mg-Nd- and Mg-Gd-Based Alloys

MENACHEM BAMBERGER, GALIT ATIYA, SUZAN KHAWALED, and ALEXANDER KATSMAN

Microstructure and phase evolution in Mg-Nd-, Mg-Gd-, and Mg-Gd-Nd-based alloys with additions of Zn, Zr, and Y were analyzed in the as-cast, solution-treated and aged conditions. Close similarity between the as-cast microstructures and precipitation sequence during aging was revealed. Along with this, distinct features of eutectic compounds and of crystal structure, composition, and orientation relationships of β'', β', and β_1 phases were established. Formation of Zn_2Zr_3 rods in Mg-Nd-based alloy and cuboid-shaped particles in Mg-Gd- and Mg-Gd-Nd-based alloys is discussed. The features of the age hardening curves were connected with differences between $\beta'' \rightarrow \beta'$ transformation and different diffusivities of Gd and Nd in Mg-matrix.

DOI: 10.1007/s11661-013-2069-0

I. INTRODUCTION

MAGNESIUM alloys containing rare earth (RE) elements have received extensive attention in recent years because of their excellent mechanical properties, especially high-temperature creep resistance, light weight, and good die-castability.[1–10] The high solid solubility of the RE elements in Mg matrix at high temperature and its substantial decrease with temperature result in remarkable age hardening response during isothermal aging at temperatures ranging from 448 to 473 K (175 to 200 °C). Among the Mg-RE systems, the Mg-Nd-, Mg-Gd-, and Mg-Gd-Nd-based alloys with small additions of Zn, Zr, and Y were believed to have considerable promising potential. While these systems have been extensively investigated, a combined effect of alloying elements on the phase evolution and the precipitation sequence is not fully understood. Microstructural characterization of the Mg-RE alloys has been performed by many researchers.[3–16] It is generally agreed that precipitation process consists of three main stages: [α-Mg supersaturated solid solution (S.S.S.S.) $\rightarrow \beta''(DO_{19}) \rightarrow \beta'$(bco) $\rightarrow \beta$(fcc)], which was recently modified by Nie and Muddle[2] to a four-stage precipitation sequence with another intermediate phase β_1(fcc) forming between β' and β phases and further confirmed by other researchers.[4,5,11,12] Among the four precipitated phases, the coherent β'' and coherent/semicoherent β' phases are considered to be the primary strengthening phases.[4,6,10,12] The yield strength or hardness usually reaches a maximum, as the materials form a microstructure with fine β' precipitates during aging.[3–6] The characteristics of these precipitates (coherency, shape, size, and density) play a significant role in the hardening effect. Detailed investigation of the phase composition and crystallographic orientation of precipitates in Mg-Nd alloys with small additions of Zn and Zr was performed by Atiya *et al.*[17–20] The investigation was continued on the Mg-Gd- and Mg-Gd-Nd-based alloys[21–23] to understand the combined effects of Nd and Gd on the precipitation sequence, the crystal orientation relationship (OR) of precipitates, exact chemical composition of the metastable phases β'', β', and β_1 and explain the corresponding microhardness curves in Mg-RE-based alloys.

II. EXPERIMENTAL

Alloys with the chemical compositions of Mg-3.1Nd-0.45Zr-0.25Zn (wt pct) were prepared by the Dead Sea Magnesium Research Institute (MRI), Mg-5Gd-0.3Zn-0.18Y-0.15Zr and Mg-6Gd-3.7Nd-0.3Zn-0.18Y-0.15Zr (wt pct) were prepared by the Technion Research & Development Foundation (TRDF). The samples were encapsulated in quartz tubes under 300 mmHg argon atmosphere and were solution treated (ST) for 24 hours at 813 K (540 °C) followed by water quenching at 298 K (25 °C). The treatment included heating to 498 K (225 °C) (heating rate of 10 °C/hour), then heating to 813 K (540 °C) at a rate of 15 °C/hour, followed by water quenching at 298 K (25 °C). Then, the samples were aged in an oil bath at 448 K (175 °C) for up to 125 days. Phase analysis was carried out using X-ray diffractometer (XRD), the microstructure was examined using optical microscopy FEI Scanning Electron Microscope (SEM), Quanta 200, and Ultra plus FEG SEM, and EDS Analysis was conducted on TEM samples with a special specimen holder to increase the reliability and ensure that the photons are scattered from a specific analyzed region. Vickers Hardness testing was performed using 50 grams load and holding time of

MENACHEM BAMBERGER, Professor, GALIT ATIYA and SUZAN KHAWALED, Ph.D. Students, and ALEXANDER KATSMAN, Senior Researcher, are with the Department of Materials Science & Engineering, Technion - Israel Institute ofTechnology, 32000 Haifa, Israel. Contact e-mail: akatsman@technion.ac.il
Manuscript submitted June 2, 2013.
Article published online October 24, 2013

15 seconds. Precipitate microstructures were examined in FEI Tecnai G2 T20 S-Twin (TEM) and FEI Titan 80-300 FEG-S/TEM (HRTEM).

III. MICROSTRUCTURE AND PHASE COMPOSITION OF Mg-Nd-BASED ALLOY

The microstructure of the Mg-3.1Nd-0.45Zr-0.25Zn (wt pct) alloy in as-cast condition (Figure 1) consists of α-Mg matrix, eutectic compounds and Zr-rich particles.[17–20]

It was revealed by SEM EDS analysis performed on the TEM sample that Zn atoms substitute Mg atoms in the eutectic compound (~2.6 at. pct). After solution treatment for 24 hours at 813 K (540 °C), only α-Mg phase was recognized from XRD data (Figure 2).[18]

However, detailed SEM and TEM investigations revealed residual eutectic compounds and Zn_2Zr_3 particles that are gathered in clusters. The aging of solution-treated samples was performed at 448 K (175 °C) up to 32 days. The microhardness increases and reaches the maximum value of about 80 HV after 8 days (Figure 3) and then decreases with the aging time.

The peak-aged sample was investigated by TEM and HRTEM (Figures 4 and 5).

TEM micrograph and corresponding SAED from grain interior indicate the presence of metastable β'' $(Mg_3Nd)_{HCP}$ (DO_{19} structure) precipitates. The precipitates have a plate-like shape and are fully coherent with the Mg matrix, with the orientation relationship (OR) $[\bar{2}110(0001)_{Mg}\|[\bar{2}110](0001)_{\beta''}$ and $[[\bar{1}010](\bar{1}2\bar{1}0)_{Mg}$ $\|[\bar{1}010](\bar{1}2\bar{1}0)_{\beta''}$. HRTEM image along $[\bar{1}010]_{Mg}$ zone axis (Figure 5) reveals β'' plate precipitate that is fully coherent with the Mg matrix.

The Zn_2Zr_3 rods, distributed in the grain interior, serve as additional nucleation sites for precipitates. The tetragonal Zn_2Zr_3 particles ($P4_2/mnm$: a = 0.768 nm and c = 0.699 nm), which seem to have a near octagon cross section (Figure 6), are elongated along [001] direction, have an orientation relationship with the Mg matrix $[[\bar{2}110](0001)_{Mg}\|[001](110)_{Zn_2Zr_3}$, and appear to be stable in the Mg matrix.

Nd-rich plate-like precipitates nucleate on the side and basal planes of the Zn_2Zr_3 as identified by EDS mounted on the TEM (Figure 7).[19] It is accompanied by the formation of precipitation-free zones (PFZs) near Zn_2Zr_3 rod particles. These plate-like precipitates were identified by SAED as $\beta_1(Mg_3Nd)(DO_3$ structure) precipitates with FCC crystal structure and lattice parameter of a = 0.739 nm. The following orientation relationships of β_1 and α-Mg were found: $[0001](2\bar{1}\bar{1}0)_{Mg}\|[101](11\bar{1})_{\beta_1}$ and $[\bar{1}010](0001)_{Mg}$ $\|[112](\bar{1}10)_{\beta_1}$ (Figure 8).[17,19]

It should be noted that this β_1 phase was mentioned as β' in our previous publications,[17–20] but after comparison with phases in Mg-Gd- and Mg-Gd-Nd-based alloys (see below), it was renamed to β_1.

A small number of large β_1 precipitates (few hundreds of nm in size) and a high density of fine β_1 precipitates were observed in the grain boundary regions. After 32 days of aging, it was found that β'' phase transforms into β_1 in the grain interior and β_1 precipitates transform into β in the grain boundary regions. In the late stage of aging, the β_1 precipitates in the matrix transform into a stable incoherent β $(Mg,Zn)_{12}Nd$ phase.

IV. MICROSTRUCTURES AND PHASE COMPOSITIONS OF Mg-Gd- AND Mg-Gd-Nd ALLOYS WITH ADDITIONS OF Zn, Y, AND Zr

Two Mg-RE alloys, Mg-5Gd and Mg-6Gd-3.7Nd with 0.3 pct of Zn, 0.18 pct of Y and 0.15 pct of Zr (wt pct), were investigated.[21–23] The microstructures of the alloys have been investigated in the as-cast condition and after solution treatment at 813 K (540 °C) for 24 hours followed by isothermal aging at 448 K (175 °C) up to 125 days by means of Vickers hardness, optical microscopy, scanning electron microscopy

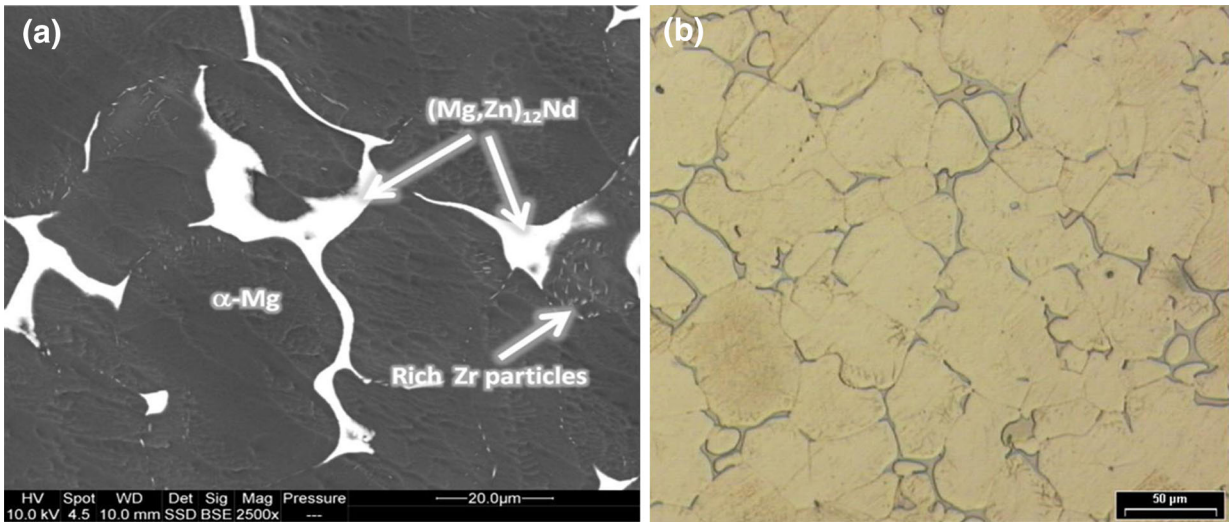

Fig. 1—(*a*) Optical micrograph and (*b*) BSE SEM micrograph of the Mg-3.1Nd-0.45Zr-0.25Zn alloy showing as-cast microstructure.

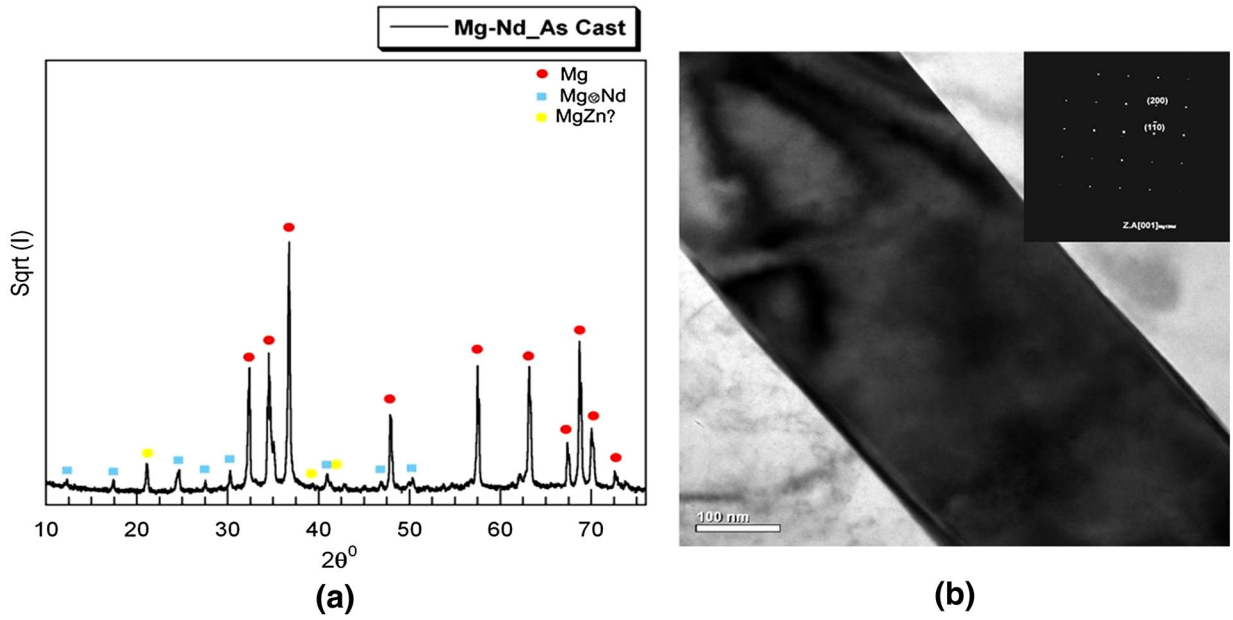

Fig. 2—(*a*) XRD patterns of the Mg-3.1Nd-0.45Zr-0.25Zn as-cast alloy; (*b*) TEM BFI and corresponding SAED of the eutectic compound zone axis $[001]_{Mg_{12}Nd}$.

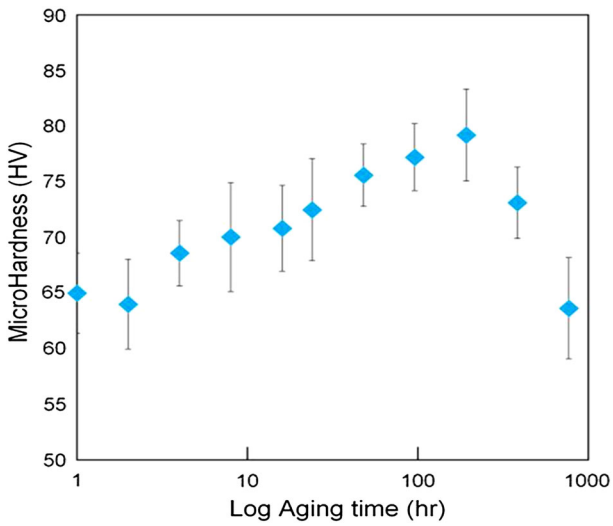

Fig. 3—Microhardness of the Mg-3.1Nd-0.45Zr-0.25Zn alloy as a function of time during isothermal aging at 448 K (175 °C).

equipped with energy dispersive X-ray spectrometry, X-ray diffraction, and transmission electron microscopy (TEM).

The microstructure of the as-cast alloys consisted mainly of the α-Mg-matrix, eutectic-like structures, cuboid-like phases, and Zr-rich clusters (Figure 9).

The cuboid-like particles in micrometer scale are frequently observed in the association with Zr-rich clusters and eutectic-like structures as shown in Figure 9. The compositions of the phases were analyzed by EDS SEM using TEM samples (Tables I and II) with SD = 0.03–1.6.

The composition of the cuboid-like particles in the as-cast Mg-5Gd-based alloy can be presented as $Gd_{0.7}(Y_xMg_{1-x})_{0.3}$ with $x = 0.5$, while in the as-cast Mg-6Gd-3.7Nd-based alloy the cuboids are Y-rich phases containing Gd and Nd with the composition $Y_{0.75}Gd_{0.25}$.

The homogenized and quenched alloys contained primary α-Mg solid solution, smaller amount of divorced eutectic compounds, enlarged cuboid-like particles, and Zr-rich clusters (Figures 10 and 11).

The compositions determined by EDS SEM analysis are presented in Table II.

The eutectic structures were the products of a "quasibinary eutectic reaction" L → α-Mg + β-Mg_5RE. The eutectic structure in the Mg-5Gd-based alloy was characterized to be α-Mg + Mg_5Gd. The microstructure of the homogenized Mg-6Gd-3.7Nd-based alloy contained skeleton-like eutectic structures (Figure 12) with the Mg_5Gd-prototype phase of the composition $Mg_5(Gd_xNd_{1-x}$, $x = 0.2)$ and FCC crystal structure.

It was found by SAED patterns that the cuboid-shaped phase has a FCC crystal structure with $a = 0.54$ nm and is a GdH_2-type compound as shown in Figure 13.

Since the EDS analysis cannot be used for the detection of element H, the compositions of the cuboid-shaped particles after homogenization (Tables I and II) are characterized by enlarged amount of Gd and can be presented $Gd_{0.7}(Y_xMg_{1-x})_{0.3}$ with $x = 0.5$ in the Mg-5Gd-based alloy, and $Gd_4(Y_xNd_{1-x})$ with $x = 0.5$ in the Mg-6Gd-3.7Nd-based alloy. The cuboid-shaped particles appeared to be stable in Mg matrix after ST, and SEM/HRSEM + EDS analysis revealed that the Gd/Nd ratio did not change during aging. The Zn_2Zr_3 (as in the Mg-3.1Nd-0.45Zr-0.25Zn alloy) or any other Zn-Zr phases were not recognized by XRD and SEM + EDS analyses.

Crystal structure of precipitates formed during aging was investigated by TEM using SAED patterns. TEM

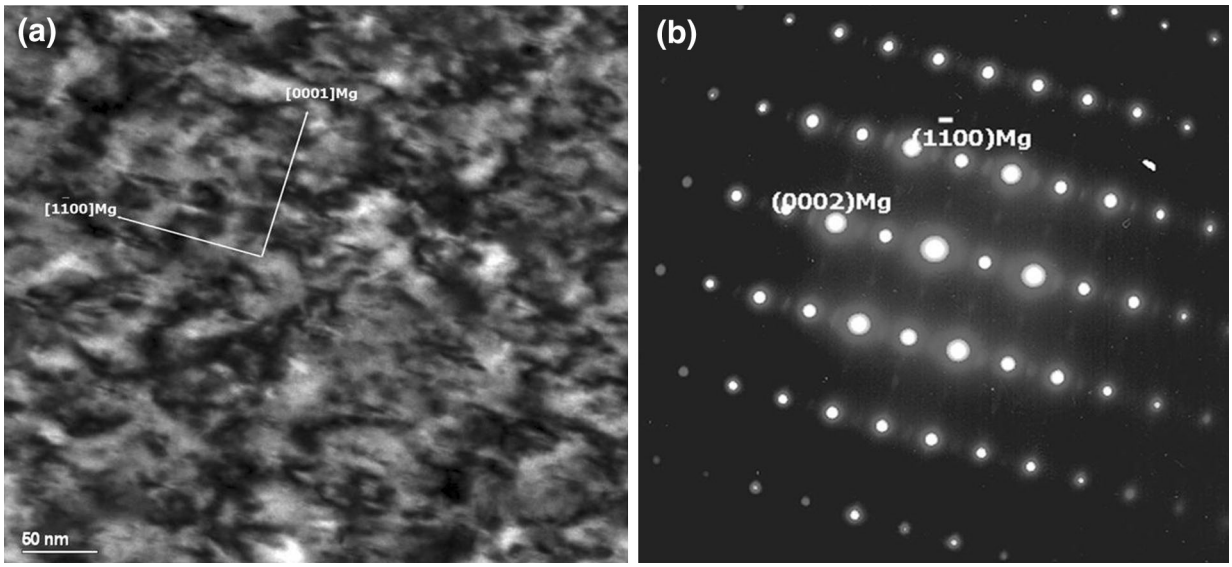

Fig. 4—(*a*) BF TEM micrograph of β'' precipitates in the Mg matrix after 8 days of aging and (*b*) corresponding SAED $[\bar{2}110](0001)_{Mg}\|[\bar{2}110](0001)_{\beta''}$.

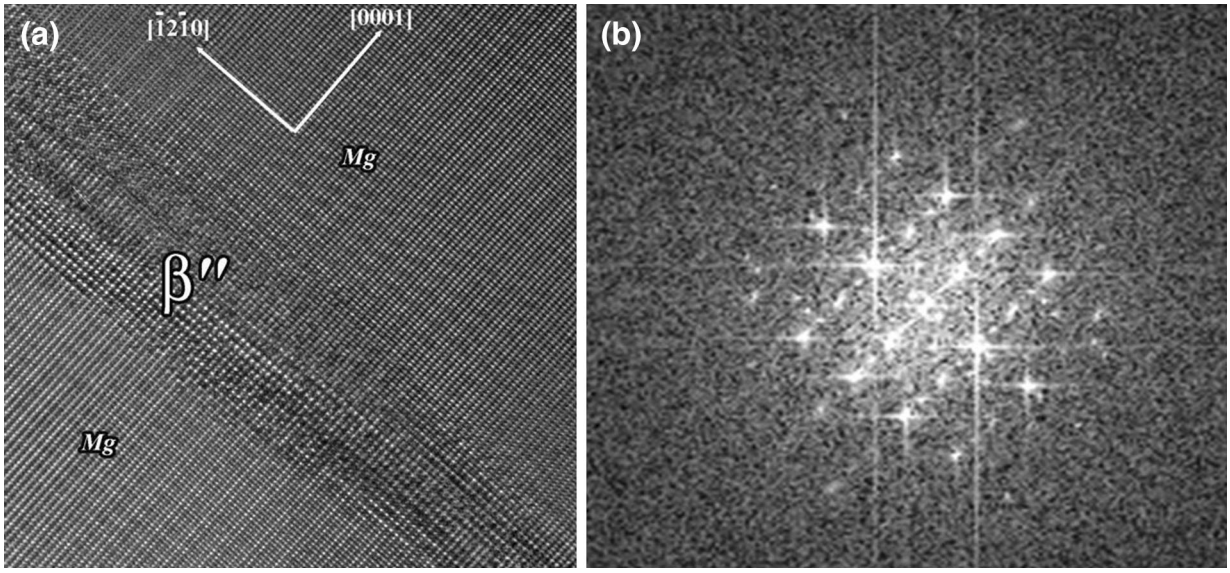

Fig. 5—(*a*) HRTEM micrograph of β'' precipitates in the Mg matrix and (*b*) corresponding fast Fourier transform (FFT) $[\bar{1}010](\bar{1}2\bar{1}0)_{Mg}\|[\bar{1}010](\bar{1}2\bar{1}0)_{\beta''}$.

image and corresponding SAED pattern of precipitates in a specimen aged for 16 hours (pre peak-aged specimen) are shown in Figure 14. It was observed that the microstructure contains a high number density of fine plate shape β'' precipitates uniformly distributed within the α-Mg matrix (Figure 14). The β'' precipitates with DO_{19} structure $\left(a \sim 2a_{\alpha-Mg} = 0.64\,\text{nm},\ c \sim c_{\alpha-Mg} = 0.52\,\text{nm}\right)$ correspond to diffuse spots at 1/2 distance of $\{01\bar{1}0\}_\alpha$ or $\{2\bar{1}\bar{1}0\}_\alpha$ reflections, with the following orientation relationships (OR) to α-Mg matrix: $[0001]_{\beta''}//[0001]_\alpha$, $\{01\bar{1}0\}_{\beta''}//\{01\bar{1}0\}_\alpha$.

The HAADF STEM image and SAED pattern typical of microstructure in Mg-Gd-Nd specimen aged for 16 days are presented in Figure 15. As seen from the image, the microstructure in the peak-aged condition contained three kinds of precipitates which can be recognized as β', β_1 phases, and very thin precipitates with few tens of nanometer size that are probably β'' precipitates.

The platelets β' have $\{\bar{2}110\}_\alpha$ habit planes and are extending along $[0001]_\alpha$ direction, while β_1 precipitates are extending along $\langle\bar{2}110\rangle_\alpha$ directions perpendicular to the $[0001]_\alpha$ axis, and $\langle\bar{2}113\rangle_\alpha$ directions with the angle of about 30 deg to the $[0001]_\alpha$ direction. As can be seen from the SAED pattern in Figure 15, the precipitate reflections are from β' and β_1 precipitates.

The following orientation relationships can be obtained:

For β' precipitates: $[100]_{\beta'}\|\ [10\bar{1}0]_{\alpha-Mg}$ and $(001)_{\beta'}\|(0001)_\alpha$;

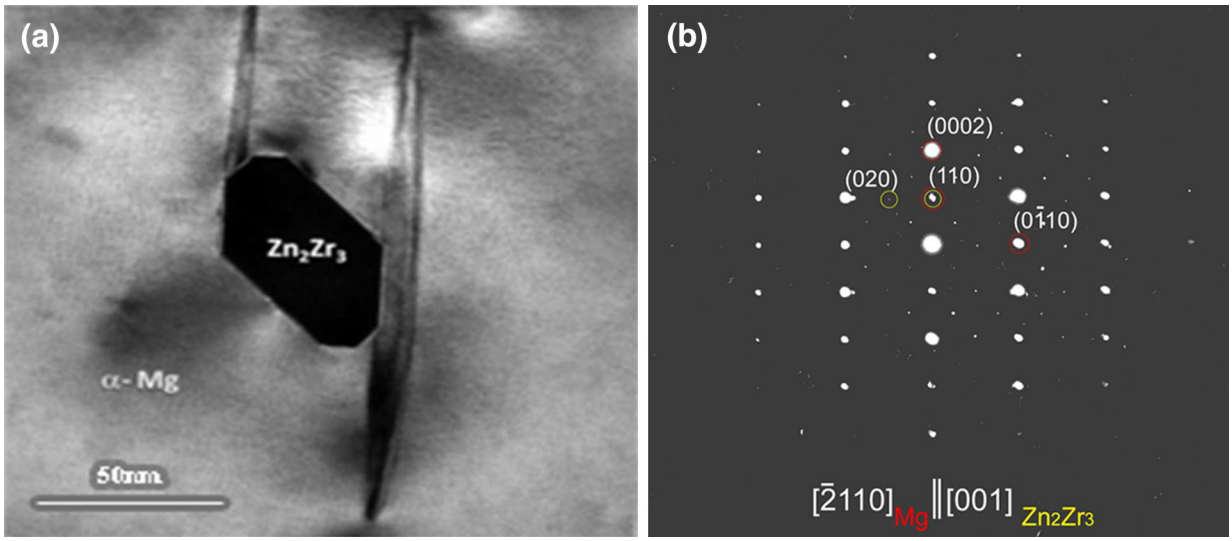

Fig. 6—BF TEM micrograph of Zn_2Zr_3 rod particle elongated to [001] direction and corresponding SAED of Mg and Zn_2Zr_3 with the OR $[\bar{2}110](0001)_{Mg} \| [001](110)_{Zn_2Zr_3}$.

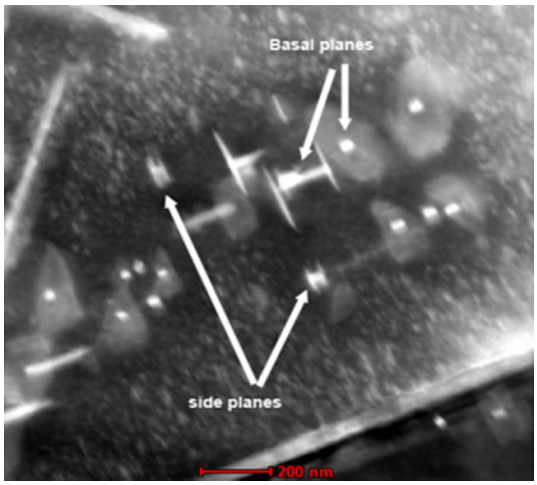

Fig. 7—DF STEM micrograph of Zn_2Zr_3 particles with Nd-rich plate-like precipitates on their basal and side planes.

For β_1 precipitates: $[112]_{\beta_1} \| [10\bar{1}0]_{\alpha-Mg}$; and $(\bar{1}10)_{\beta_1} \| (0001)_{\alpha}$.

Typical high angle annular dark-field (HAADF) STEM image and corresponding SAED pattern of the Mg-Gd-Nd-based alloy specimen aged for 32 days are shown in Figure 16. As can be seen, the microstructure contained β' and β_1 precipitates, while β_1 precipitates appear often to be associated with β' precipitate.

β' precipitates are elongated along $[0001]_{\alpha}$ direction, while β_1 precipitates are elongated along two directions which are apparently the projections of $\langle \bar{2}113 \rangle_{\alpha}$ directions on the $(2\bar{1}\bar{1}0)_{\alpha}$ plane.

The OR $[100]_{\beta'} \| [111]_{\beta_1}$, $(00\bar{2})_{\beta'} \| (20\bar{2})_{\beta_1}$ between β' and β_1 precipitates with very small lattice mismatch can allow for nucleation of β_1 on the β' precipitates (Figure 16).

After aging for 64 days, the β' precipitates almost totally transformed to platelet β_1 precipitates. The typical microstructure (TEM image) and corresponding SAED pattern of Mg-Gd-Nd alloy specimen aged for 64 days (Figure 17) show that the platelet β_1 precipitates are elongated along three equivalent directions of $\langle \bar{2}110 \rangle_{\alpha}$ with habit planes $\{10\bar{1}0\}_{\alpha}$. The angles between the variants are 60 or 120 deg.

The OR between β_1 precipitate and the matrix is $[101]_{\beta_1} \| [0001]_{\alpha-Mg}$ and $(11\bar{1})_{\beta_1} \| (11\bar{2}0)_{\alpha}$, which, in fact, is the same as mentioned above.

In 448 K (175 °C)/125 day-aged specimen of the Mg-Gd-Nd-based alloy, the microstructure contained long needle-like precipitates much coarser than those observed in 448 K (175 °C)/64 days aged specimen (Figure 18).

These precipitates seem to grow from the eutectic structure as the continuation of its β phase in the process of coarsening when the smaller β_1 and β precipitates presented in the α-Mg matrix are dissolved. The β phase has a crystal lattice with FCC (a = 2.22 nm) structure and composition of Mg_5RE.

A. *Microhardness*

The microhardness evolution of the Mg-5Gd and Mg-6Gd-3.7Nd-based alloys during isothermal aging at 448 K (175 °C) up to 125 days with error bars of ±3HV is shown in Figure 19. This shows that the Mg-5Gd-based alloy displays a two-stage behavior typical for Mg-Gd alloys.[24]

In the first stage, the microhardness increased and, after 2 days of aging, reached a first maximum, then it slightly decreased, and increased again up to a second maximum value after ~16 to 64 days of aging. Further aging led to a decline in the microhardness. During aging of Mg-6Gd-3.7Nd-based alloy, the microhardness reached a first maximum (of about 90 HV) after 8 hours, then it decreased, but, after 16 hours, increased again until reaching a second maximum (~100 HV) after 2 days of aging; the third peak was reached after

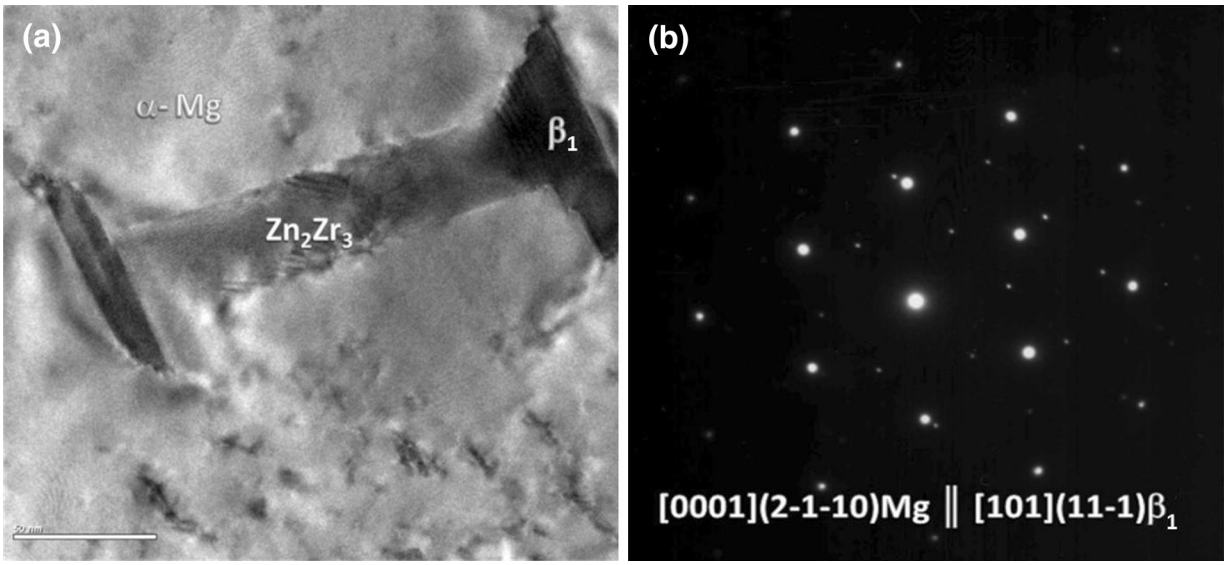

Fig. 8—(*a*) TEM micrograph and (*b*) corresponding SAED of β_1 precipitate nucleated on Zn_2Zr_3 rod particle.

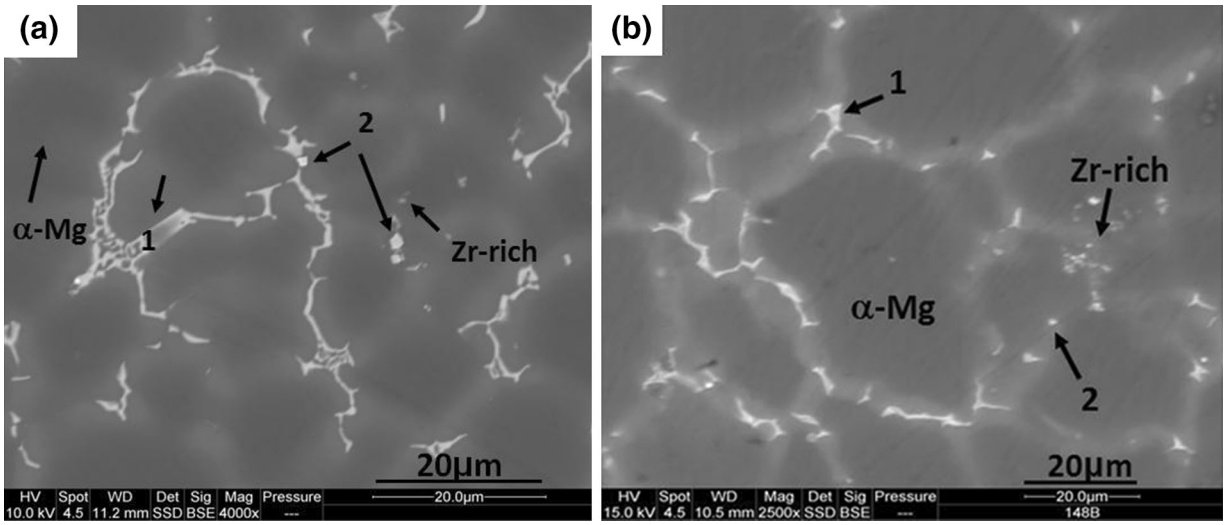

Fig. 9—Microstructures of TEM specimens of the as-cast samples for Mg-6Gd-3.7Nd-based alloy (*a*) and Mg-5Gd-based alloy (*b*). SEM images show eutectic-like structure (1) and cuboid-like phase (2).

Table I. Compositions of Different Phases in Mg-5Gd-based Alloy Measured by EDS SEM

Mg-5Gd	Mg (at. pct)	Gd (at. pct)	Y (at. pct)	Zr (at. pct)	Phase
As-cast	99.01	0.52	0.14	0.15	α-Mg
	82.43	17	0.53	0.0	eutectic
	13.08	73.96	12.96	0.0	cuboid
	89.27	4.7	2.37	3.69	Zr rich
ST	98.98	0.68	0.11	0.18	α-Mg
	93.95	5.58	0.52	0.0	eutectic
	13.41	74.42	11.97	0.2	cuboid
	82.19	3.57	2.89	11.32	Zr rich
16 days	99.17	0.82	0.0	0.14	α-Mg
	93.22	5.54	0.77	0.47	eutectic
	12.65	75.62	11.72	0.01	cuboid
	94.33	0.61	0.0	5.12	Zr rich

Table II. Compositions of Different Phases in Mg-Gd-Nd-Based Alloy Measured by EDS SEM

Mg-6Gd-3.7Nd	Mg (at. pct)	Gd (at. pct)	Nd (at. pct)	Y (at. pct)	Zr (at. pct)	Phase
As-cast	99.06	0.42	0.21	0.14	0.16	α-Mg
	84.82	7.43	7.73	0.0	0.0	eutectic
	9.09	22.63	0.90	67.37	0.0	cuboid
	94.03	1.51	0.76	0.0	3.7	Zr rich
ST	98.18	0.94	0.54	0.12	0.22	α-Mg
	89.21	2.29	8.53	0.0	0.0	eutectic
	10.36	69.13	11.66	8.85	0.0	cuboid
	92.1	1.51	0.4	0.61	5.38	Zr rich
16 days	98.5	0.99	0.63	0.0	0.0	α-Mg
	88.8	2.06	9.11	0.0	0.0	eutectic
	3.11	75.22	10.7	10.96	0.0	cuboid
	86.57	2.47	0.0	0.09	10.95	Zr rich

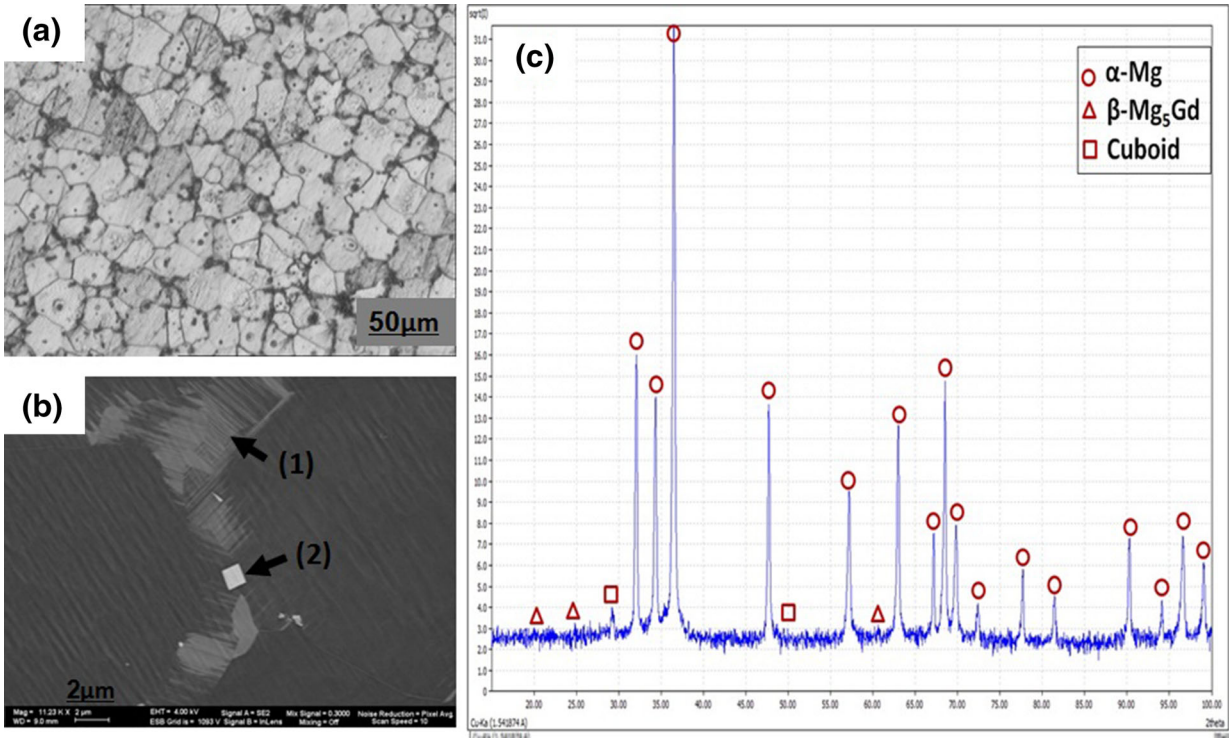

Fig. 10—Microstructure of the ST Mg-5Gd-based alloy (*a*) optical image and (*b*) SEM image showing the eutectic structure (1) and cuboid-shaped phase (2). (*c*) X-ray diffraction.

~16 days of aging. Further aging resulted in the decrease of the microhardness.

V. DISCUSSION

The microstructure of the as-cast Mg-RE-based alloys was similar for the Mg-Nd- and Mg-Gd-based alloys: it consists of α-Mg matrix, eutectic compounds, and Zr-rich particles. The presence of Y in Mg-Gd-based alloys led to formation of cuboid-shaped particles containing Y, Gd, Nd, and Mg. However, the eutectic compounds are different: for the case of Mg-3.1Nd-based alloy, the compound is $Mg_{12}Nd$ where Zn atoms may substitute Mg atoms (up to ~2.6 at. pct); for the case of Mg-5Gd and Mg-6Gd-3.1Nd-based alloys, it is Mg_5Gd-prototype phase of the composition $Mg_5(Gd_xNd_{1-x})$ with $x = 1$ for the first alloy and $x = 0.5$ for the second one. After solution treatment followed by water quenching, supersaturated solution of RE metals in the Mg-matrix was attained. Besides, the Zn_2Zr_3 particles formed in the grain interior of the ST Mg-3.1Nd-0.45Zr-0.25Zn alloy, while no Zn-Zr phases were found in the ST Mg-5Gd-0.3Zn-0.18Y-0.15Zr and Mg-6Gd-3.7Nd-0.3Zn-0.18Y-0.15Zr alloys. The absence of Zn_2Zr_3 phase in the two last alloys may be connected with higher Zn solubility in the Mg-Gd matrix compared with Mg-Nd or pure α-Mg matrix (or/and with smaller amount of Zr there). The Zn_2Zr_3 rods influence on the precipitation of metastable phases during aging, with these rods providing additional places for nucleation of these phases.

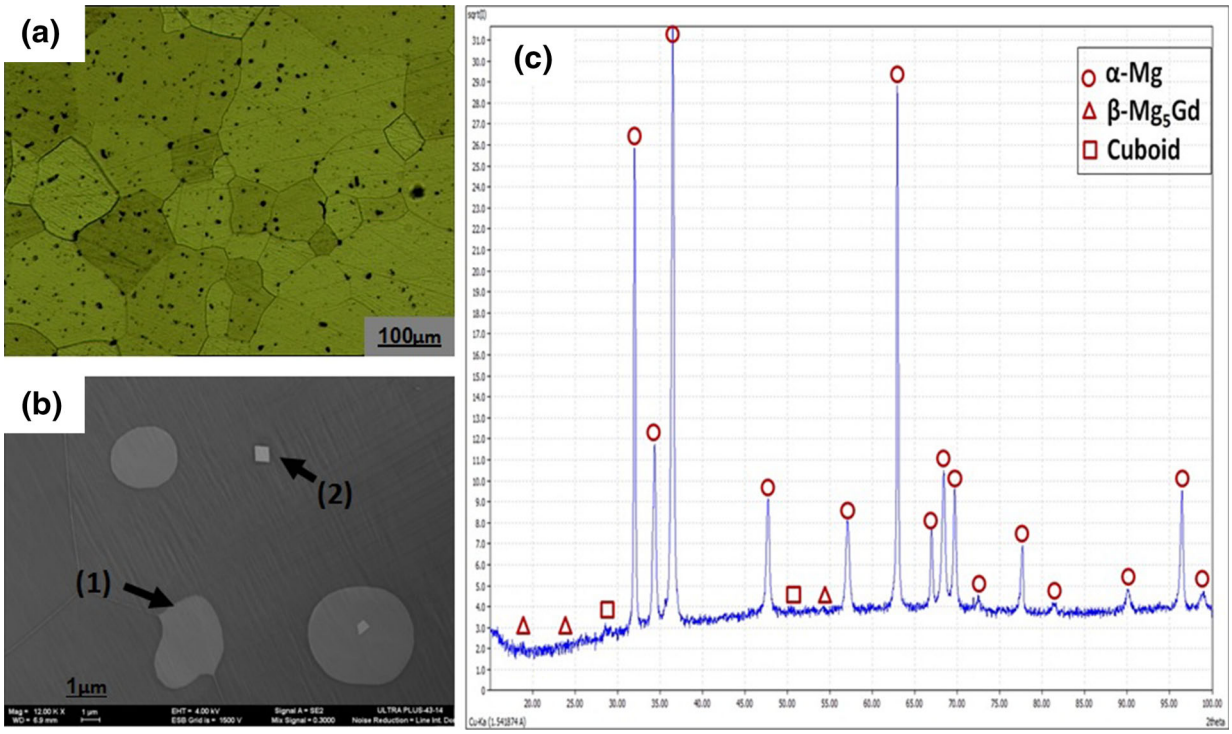

Fig. 11—Microstructure of the ST Mg-6Gd-3.7Nd-based alloy (*a*) optical image and (*b*) SEM image showing the eutectic structure (1) and cuboid-shaped phase (2). (*c*) X-ray diffraction.

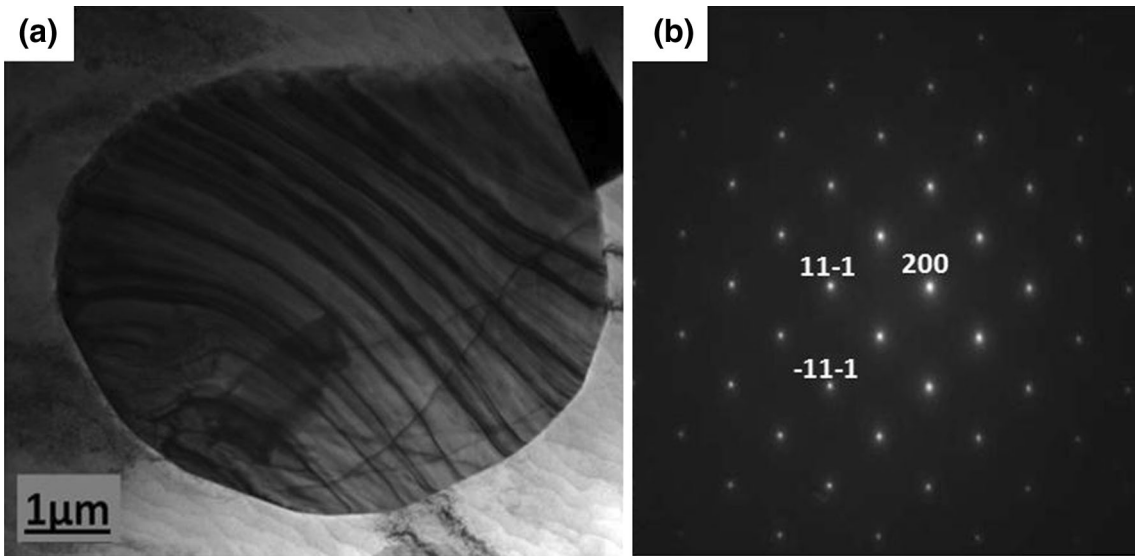

Fig. 12—(*a*) BF TEM micrograph of the ST Mg-Gd-Nd alloy eutectic phase from the ST sample and (*b*) corresponding SAED pattern of the sample in zone axis [011], identifying Mg_5RE cubic eutectic phase.

Formation of the cuboid-shaped particles in the Mg-RE-based alloys has been investigated in a number of studies.[6,25] They were identified to have a fcc crystal structure (a = 0.56 nm), and the composition depending on the alloy constitution and thermal treatment conditions. Zheng *et al.*[6] assumed that these are the RE-hydrides of the GdH_2 type. Since the hydrogen canot be detected by EDS analysis, a hydride may be assumed for a cuboid-shaped phase. (GdH_2 compound has a fcc structure with a = 0.5303 nm; different compositions of the cuboid phases can be obtained if part of Gd atoms is replaced by Nd, Y or Mg).

Formation of cuboid-shaped particles in the investigated Mg-Gd- and Mg-Gd-Nd-based alloys was connected with the presence of Y and Gd—all the cuboid-shaped particles in the as-cast condition contained

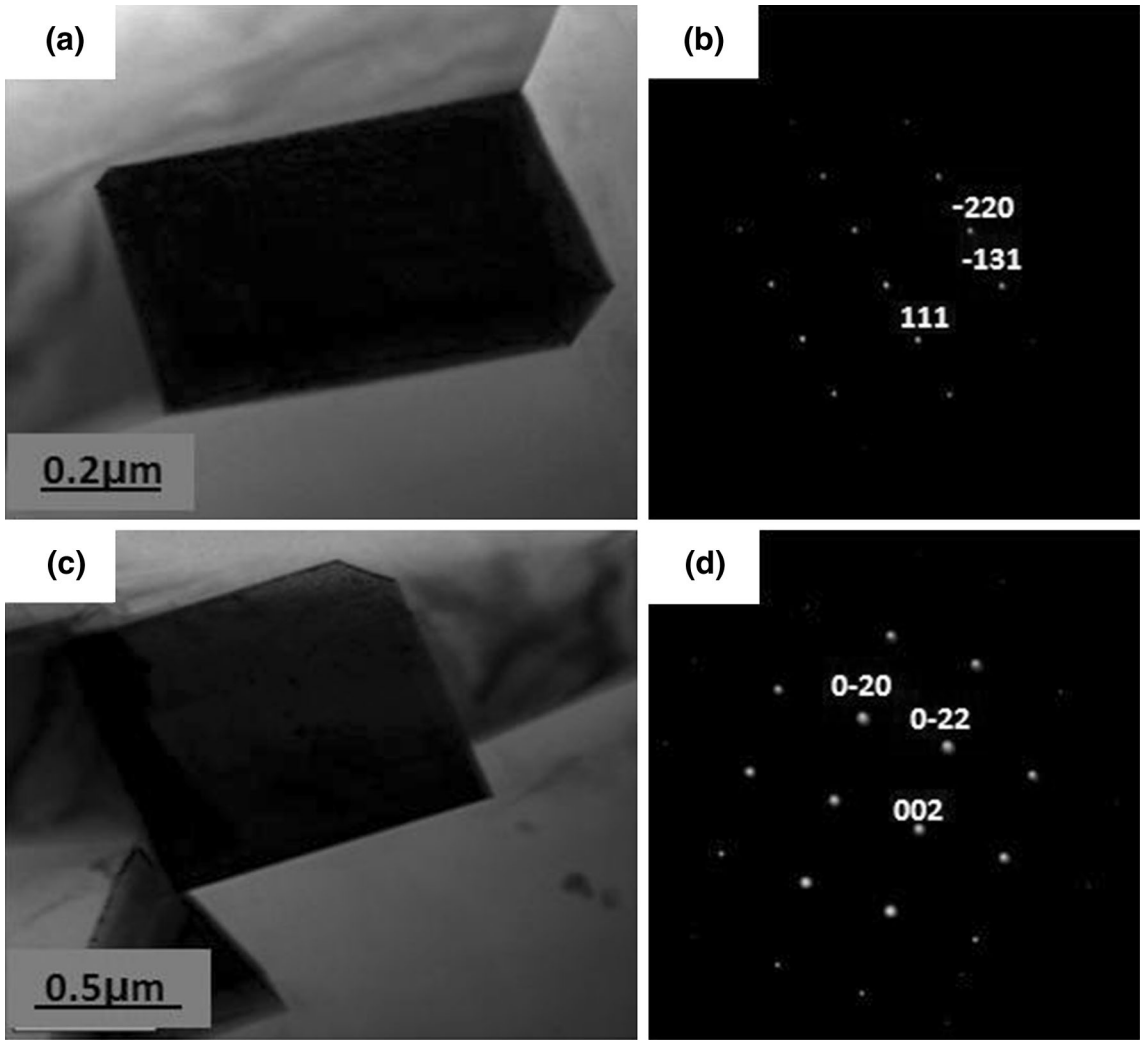

Fig. 13—BF TEM micrograph of the ST Mg-Gd-Nd alloy with cuboid-shaped phase and corresponding SAED patterns with zone axes $[\bar{1}\bar{1}2]$ in (*a, b*) and [100] in (*c, d*).

enlarged amount of Y and Gd. One can assume that the Y and/or Gd hydrides formed during melting or casting. YH_2 phase has a fcc crystal structure with $a = 0.525$ nm. Part of yttrium atoms can be replaced by Gd, Nd, and Mg. In the as-cast Mg-5Gd-based alloy, the Gd atoms in the RE-hydride (*e.g.*, GdH_2 phase) were partially replaced by Y and Mg to form the compound $Gd_{0.7}(Y_xMg_{1-x})_{0.3}$, with $x = 0.5$, this phase was found to be stable during ST applied. In the as-cast Mg-6Gd-3.7Nd-based alloy, the RE elements in the REH_2-type compound were mainly Y and Gd with relative composition of $Y_{0.75}Gd_{0.25}$.

It was found from SAED patterns after ST (Figures 13(b) and (d)) that the cuboid-shaped phase has a FCC crystal structure with $a = 0.54$ nm corresponding to a GdH_2-type compound. The heat treatment caused diffusion of Gd and Nd atoms in α-Mg matrix toward the cuboid-like phases and partial replacement of Y by Gd and Nd atoms resulting in relative composition of $Gd_4(Y_xNd_{1-x})$ with $x = 0.5$. After ST, the cuboid-shaped particles appeared to be stable during aging at 448 K (175 °C) that corresponds to stability of RE hydrides at this temperature. SEM/HRSEM + EDS analysis revealed that the Gd/Nd ratio did not change during aging.

Decomposition of supersaturated solid solution during aging resulted in the precipitation of coherent plate-shaped $\beta''(DO_{19})$ phase with the composition Mg_3RE. The β'' phase then may transform to the β' phase with the composition Mg_7RE and the base-centered orthorhombic (BCO) crystal structure ($a \sim 2a_{\alpha\text{-Mg}} = 0.64$ nm, $b \sim 2.2$ nm, and $c \sim c_{\alpha\text{-Mg}} = 0.52$ nm)[26] as in the Mg-Gd and Mg-Gd_Nd-based alloys. The β' precipitates have a few hundreds of nanometers platelet-like shape in habit planes $\{\bar{2}110\}_{\alpha-Mg}$ and grow along $\langle 0001\rangle_{\alpha-Mg}$. It was found that β' precipitates are coherent with the Mg matrix, with the following orientation relationship: $[10\bar{1}0](0001)_{\alpha-Mg}\|[100](001)_{\beta'}$. At the next stage of aging, β' transforms to a semicoherent $\beta_1(DO_3)$ phase with the composition Mg_3RE and FCC ($a = 0.74$ nm) structure. In the investigated Mg-Nd-based alloy, β'' transformed directly to the β_1 phase.

The β_1 precipitates have a hundreds of nanometers platelet-like shape in habit planes $\{0\bar{1}10\}_{\alpha-Mg}$, grew mainly

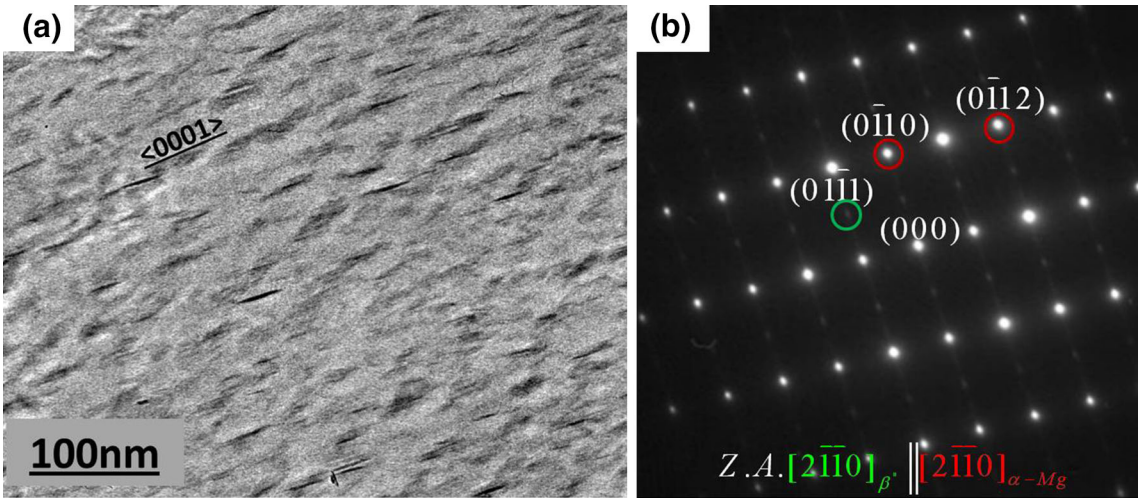

Fig. 14—(*a*) TEM image and (*b*) corresponding SAED pattern of Mg-Gd-Nd alloy aged for 16 h at 448 K (175 °C); zone axis $[\mathbf{2110}]_{\alpha}$.

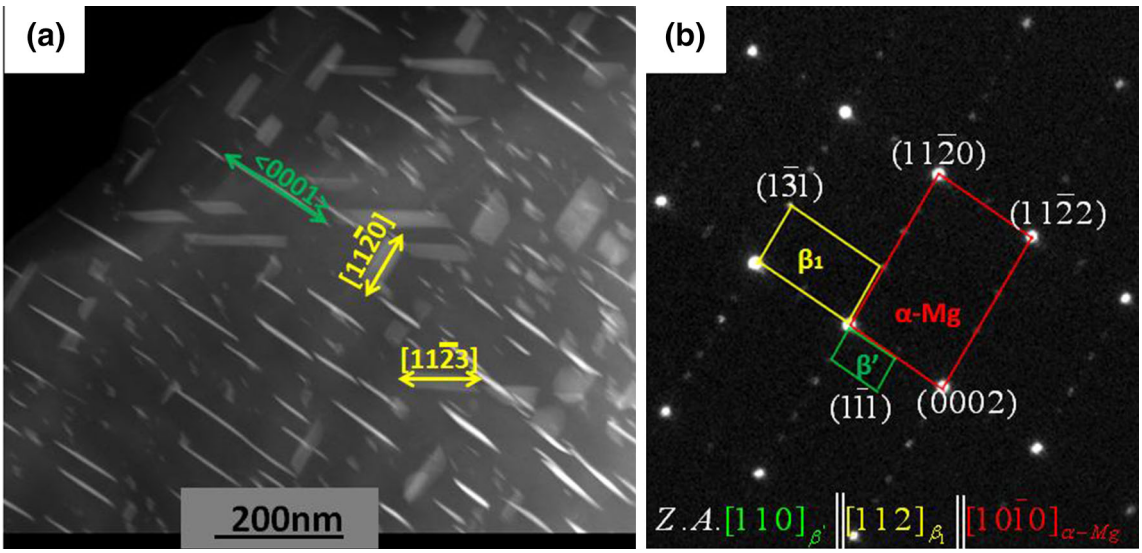

Fig. 15—(*a*) HAADF STEM image and (*b*) corresponding SAED pattern of Mg-Gd-Nd alloy aged for 16 days at 448 K (175 °C); zone axis $[\mathbf{1010}]_{\alpha}$.

along three directions of $\langle 11\bar{2}0\rangle_{\alpha-Mg}$ and are semicoherent with the α-Mg matrix, with the following orientation relationship: $[110]_{\beta_1} \| [0001]_{\alpha}$ and $(1\bar{1}1)_{\beta_1} \| (11\bar{2}0)_{\alpha}$.

OR of the $\beta_1(Mg_3RE)_{FCC}$ with the α-Mg matrix provides small lattice misfits in $[0001]_{\alpha}$ directions (0.31 pct), but rather large misfits in $[\bar{2}110]_{\alpha}$ directions (11.4 pct).[17] This explains why the β_1 precipitates are semicoherent. Another situation is realized for the bco β' in the α-Mg matrix: in $[0001]_{\alpha}$ directions lattice misfits are small ($c_{\beta'} \sim c_{\alpha-Mg}$), in $[\bar{2}110]_{\alpha}$ and $[\bar{1}010]_{\alpha}$ directions they are also small ($a_{\beta'} \sim 2a_{\alpha-Mg}$ and $b_{\beta'} \sim 8d_{[\bar{1}010]\alpha-Mg}$). Thus, bco β' can be coherent with α-Mg matrix.

At the overaging stage, metastable phases transform to a stable incoherent β phase ($Mg_{12}Nd$ in the Mg-Nd-based alloys and Mg_5Gd in the Mg-Gd- and Mg-Gd-Nd-based alloys).

The presence of two age hardening peaks in the Mg-Gd-based alloys, compared with one peak in the Mg-Nd-based alloy, testifies the intermediate transformation $\beta'' \rightarrow \beta'$ which was absent in the Mg-Nd-based alloy. Formation of β' phase with the composition Mg_7RE involves additional Mg atoms from the adjacent Mg matrix. It increases precipitated volume and precipitates' average size and, by these means, provides additional increase of microhardness. Transformation $\beta' \rightarrow \beta_1$ results in decrease of precipitates' volume and corresponding decrease of microhardness after the second or third maximum in the Mg-Gd- and Mg-Gd-Nd-based alloys, respectively. Heterogeneous nucleation of β_1 phase on the Zn_2Zr_3 rods may explain early formation of this phase in the Mg-Nd-based alloy, while in the Mg-Gd- and Mg-Gd-Nd-based alloys, it nucleates heterogeneously on the β' precipitates.

Nucleation and growth of Mg-RE phases are controlled by diffusion of RE elements in Mg matrix. Experimental values for RE diffusion in Mg are very

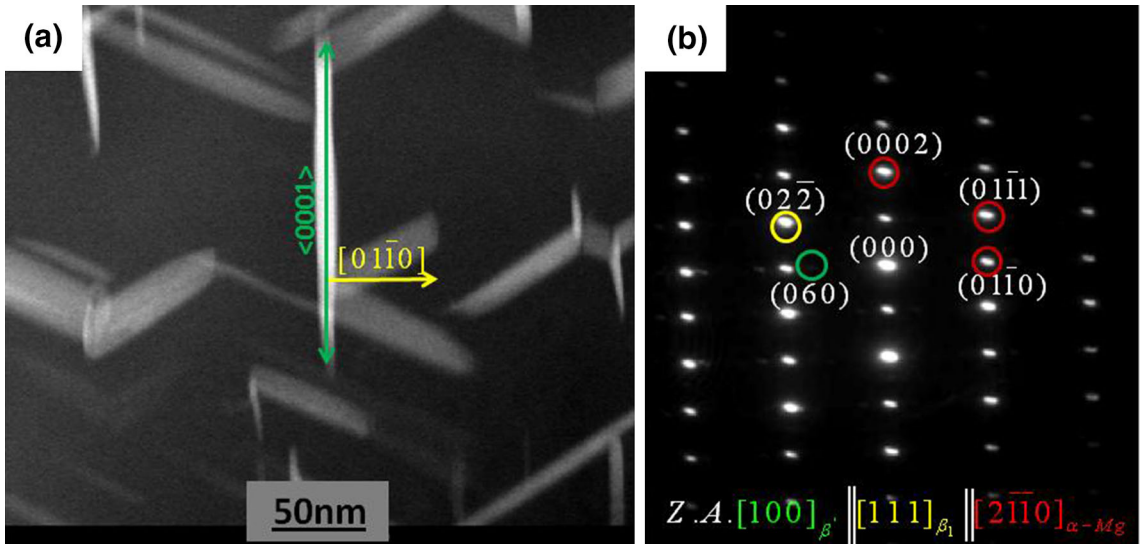

Fig. 16—(*a*) HAADF STEM image and (*b*) corresponding SAED pattern of Mg-Gd-Nd alloy aged for 32 days at 448 K (175 °C); zone axis $[\mathbf{2\bar{1}\bar{1}0}]_{\alpha}$.

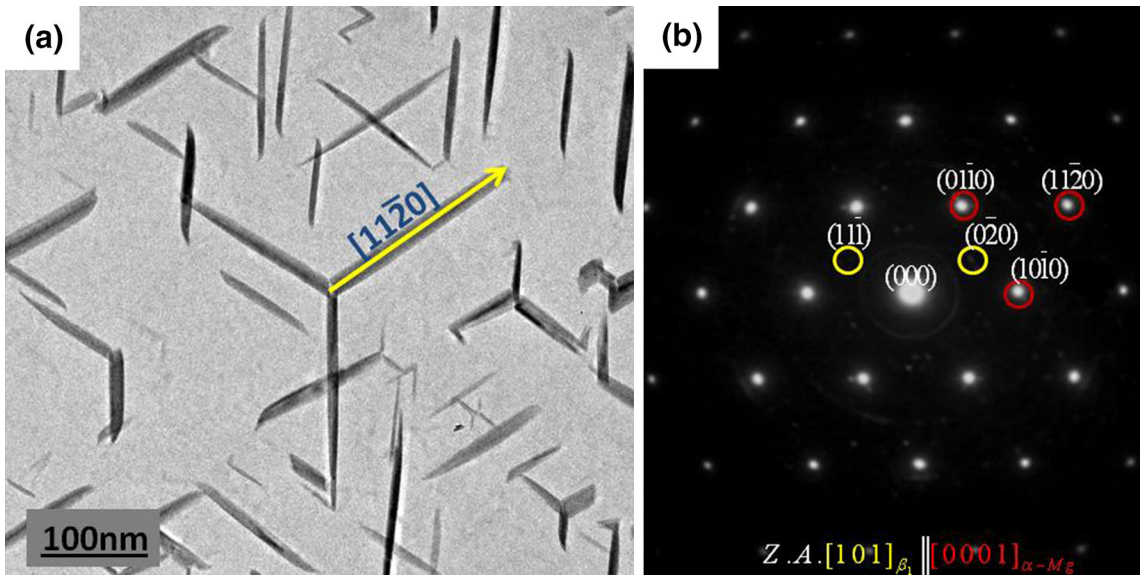

Fig. 17—(*a*) TEM image and (*b*) corresponding SAED pattern of Mg-Gd-Nd alloy aged for 64 days at 448 K (175 °C); zone axis $[0001]_{\alpha}$.

limited. Ab initio calculations of diffusion of several RE impurities in Mg were performed recently by Huber *et al.*[27] For Nd and Gd, they obtained the diffusion activation energies of 1.05 and 1.17 eV, respectively. Assuming the equal pre-exponential factors, the ratio of diffusion coefficients of Nd and Gd at 448 K (175 °C) can be estimated as $D_{Nd}/D_{Gd} = \exp(0.12\ \text{eV/kT}) \sim 20$. One can assume that the first peak in the Mg-Gd-Nd-based alloy corresponds to formation of β'' that contain mainly Nd (Mg_3Nd phase), while the second peak (first peak in the Mg-Gd-based alloy)—after 2 days of aging, resulted from the diffusion of Gd to form β'' precipitates containing Nd and Gd. In the coarsening regime (the overaging stage), the precipitate number density, N_V, decreases with time, $N_V^{-1} \sim \alpha_{LSW} t \sim D_{RE} t$, where α_{LSW} is the coefficient of the LSW-coarsening theory. The microhardness roughly is inversely proportional to a distance between precipitates,[28] and thus, is proportional to $N_V^{1/3}$. Therefore, one can expect that the overaging stage in the Mg-Gd alloys would be substantially longer (to $\sim 20^{1/3} = 2.7$ times) than in the Mg-Nd alloys. The microhardness curves for Mg-Nd- and Mg-Gd-based alloys (Figures 3 and 14) confirm this evaluation.

VI. CONCLUSIONS

Comparison study of phase evolution in Mg-RE alloys revealed close similarity of the alloys microstructure and precipitation sequence during aging among Mg-Nd-, Mg-Gd-, and Mg-Gd-Nd-based alloys. Along with this, on closer investigation of crystal structure,

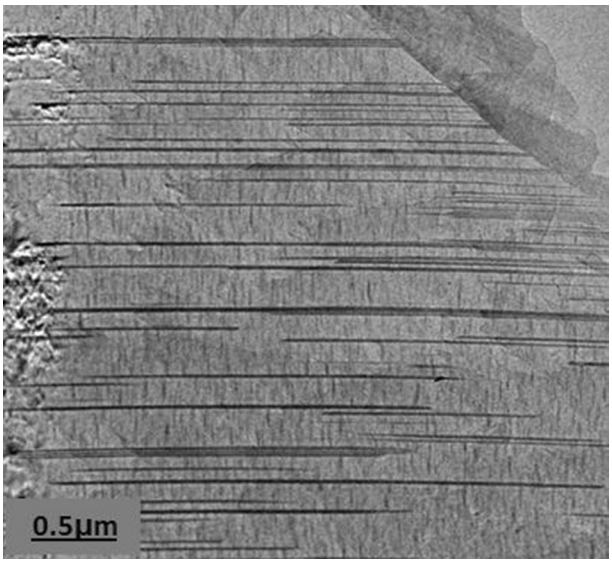

Fig. 18—TEM image of Mg-Gd-Nd alloy aged for 125 days at 448 K (175 °C), showing needle-like β precipitates.

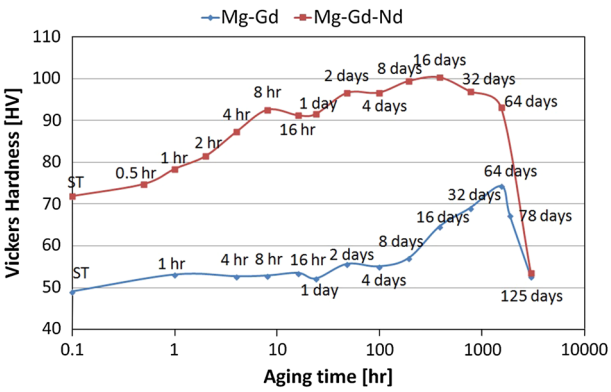

Fig. 19—Age hardening curves of the Mg-6Gd-3.7Nd and Mg-5Gd-based alloys aged at 448 K (175 °C).

composition, and OR of metastable phases β'', β', and β_1, certain distinct features emerged. These features are connected with different structures of eutectic compounds and of final stable phases β ($Mg_{12}Nd$ and Mg_5Gd, respectively), and with the formation of additional metastable β' phase in the Mg-Gd- and Mg-Gd-Nd-based alloys. Transformation $\beta'' \rightarrow \beta_1$ provides one age hardening peak in the Mg-Nd-based alloy.

Transformations $\beta'' \rightarrow \beta' \rightarrow \beta_1$ in the Mg-Gd- and Mg-Gd-Nd-based alloys are manifested in two age hardening peaks. The first peak is connected with formation of $\beta''(Mg_3RE)$ phase which, in turn, is divided in the Mg-Gd-Nd-based alloy into two subpeaks associated with the formation of $\beta''(Mg_3Nd)$ and $\beta''(Mg_3(GdNd))$ phases. The second microhardness peak is connected with transformation $\beta' \rightarrow \beta_1$. Slower diffusion of Gd in Mg matrix (in comparison with Nd) provided a longer overaging stage in Mg-Gd-based alloys. Formation of Zn_2Zr_3 rods, distributed in the grain interior of Mg-Nd-based alloy and served as additional nucleation sites for precipitates, resulted in early heterogeneous nucleation of β_1 phase and formation of T-like and H-like particles. The absence of Zn-Zr phases in the investigated Mg-Gd- and Mg-Gd-Nd-based alloys can be connected with higher solubility of Zn in the Mg-Gd matrix comparing to Mg-Nd matrix. The cuboid-shaped particles found in the Mg-Gd-and Mg-Gd-Nd-based alloys were the Y- and Gd-containing phases with the composition changing during ST, but nearly constant during aging. It was assumed that these particles are the fcc YH_2-type hydrides where Y atoms can be replaced by Gd, Nd, and Mg. The cuboid-shaped particles are stable during aging at 448 K (175 °C).

REFERENCES

1. T.J. Pike and B. Noble: *J. Less Common Metals*, 1973, vol. 30, pp. 63–74.
2. J.F. Nie and B.C. Muddle: *Acta Mater.*, 2000, vol. 48, pp. 1691–1703.
3. K.Y. Zheng, J. Dong, X.Q. Zeng, and W.J. Ding: *Mater. Sci. Eng.*, 2008, vol. 489A, pp. 44–54.
4. F. Penghuai, P. Liming, J. Haiyan, M. Lan, and J. Chunquan: *Mater. Sci. Eng. A*, 2008, vol. 496 (1–2), pp. 177–88.
5. P.J. Apps, H. Karimzadeh, J.F. King, and G.W. Lorimer: *Scripta Mater.*, 2003, vol. 48, pp. 1023–28.
6. K.Y. Zheng, J. Dong, X.Q. Zeng, and W.J. Ding: *Mater. Sci. Technol.*, 2008, vol. 24 (3), pp. 320–26.
7. S.M. He, X.Q. Zeng, L.M. Peng, X. Gao, J.F. Nie, and W.J. Ding: *J. Alloys Compd*, 2007, vol. 427, pp. 316–23.
8. K.Y. Zheng, X.Q. Zeng, J. Dong, and W.J. Ding: *Mater. Sci. Eng. A*, 2008, vol. 492, pp. 185–90.
9. L. Gao, R.S. Chen, and E.H. Han: *J. Mater. Sci.*, 2009, vol. 44, pp. 4443–54.
10. K.Y. Zheng, J. Dong, X.Q. Zeng, and W.J. Ding: *Trans. Nonferrous Met. Soc.* China, 2007, vol. 17, pp. 1164–68.
11. D. Li, J. Dong, X.Q. Zeng, C. Lu, and W.J. Ding: *J. Alloys Compd*, 2007, vol. 439, pp. 254–57.
12. K.Y. Zheng, J. Dong, X.Q. Zeng, and W.J. Ding: *Mater. Sci. Eng. A*, 2008, vol. 491, pp. 103–09.
13. K.Y. Zheng, J. Dong, X.Q. Zeng, and W.J. Ding: *Mater. Sci. Eng. A*, 2007, vol. 454–455, pp. 314–21.
14. K.Y. Zheng, J. Dong, X.Q. Zeng, and W.J. Ding: *Mater. Charact.*, 2008, vol. 59, pp. 857–62.
15. K.Y. Zheng, J. Dong, X.Q. Zeng, and W.J. Ding: *Mater. Sci. Eng. A*, 2008, vol. 489, pp. 44–54.
16. G. Sha, J.H. Li, W. Xu, K. Xia, W.Q. Jie, and S.P. Ringer: *Mater. Sci. Eng. A*, 2010, vol. 527, pp. 5092–99.
17. G. Atiya: Research Thesis for M.Sc., Technion Israel, 2011, Adar 5771.
18. G. Atiya, M. Bamberger, and A. Katsman: *Mater. Sci. Forum*, 2011, vol. 690, pp. 218–21.
19. G. Atiya, M. Bamberger, and A. Katsman: *Magnesium Technology 2011*, W.H. Sillekens, S.R. Agnew, N.R. Neelameggham, and S.N. Mathaudhu, eds., TMS Proc., San Diego, CA, USA, February 27–March 3, 2011, pp. 249–53.
20. G. Atiya, M. Bamberger, and A. Katsman: *Int. J. Mater. Res.*, 2012, vol. 10, pp. 1277–80.
21. S. Khawaled, M. Bamberger, and A. Katsman: *Mg Technology 2012*, S.N. Mathaudhu, W.H. Sillekens, N.R. Neelameggham, and N. Hort, eds., TMS 2012 Annual Meeting, Orlando, FL, March 11–15, 2012, pp. 465–68.
22. S. Khawaled, M. Bamberger, and A. Katsman: *Microstructure and Phase Composition of Homogenised and Aged Mg-Gd and Mg-Gd-Nd Alloys with Additions of Zn, Y and Zr*, Proceedings of the XXI International Materials Research Congress, Cancun, August 12–17, 2012.
23. S. Khawaled, M. Bamberger, and A. Katsman: *Magnesium Technology 2013*, N. Hort, S.N. Mathaudhu, and N.R. Neelameggham, March 3–7, 2013, San Antonio, TX, pp. 357–62.
24. T. Kawabata, K. Matsuda, and S. Ikeno: *Mater. Trans.*, 2010, vol. 51 (2), pp. 301–04.

25. S.M. He, X.Q. Zeng, L.M. Peng, X. Gao, J.F. Nie, and W.J. Ding: *J. Alloys Compd*, 2007, vol. 427, pp. 316–23.
26. M. Nishijima, K. Hiraga, M. Yamasaki, and Y. Kawamura: *Mater. Trans.*, 2006, vol. 47 (8), pp. 2109–12.
27. L. Huber, I. Elfimov, J. Rottler, and M. Militzer: *Phys. Rev. B*, 2012, vol. 85, pp. 144301-1–144301-7.
28. A. Katsman, S. Cohen, and M. Bambereger: *J. Mater. Sci.*, 2007, vol. 42 (16), pp. 6996–7003.